Monthly Notices
of the
ROYAL ASTRONOMICAL SOCIETY

MNRAS **438,** 307–317 (2014)
Advance Access publication 2013 December 13

doi:10.1093/mnras/stt2183

Revisiting the proposed circumbinary multiplanet system NSVS 14256825

Tobias Cornelius Hinse,[1]⋆ Jae Woo Lee,[1] Krzysztof Goździewski,[2] Jonathan Horner[3] and Robert A. Wittenmyer[4]

[1]*Korea Astronomy and Space Science Institute, Daejeon 305-348, Republic of Korea*
[2]*Nicolaus Copernicus University, Torun Centre for Astronomy, PL-87-100 Torun, Poland*
[3]*School of Physics, University of New South Wales, Sydney, NSW 2052, Australia*
[4]*Australian Centre for Astrobiology, University of New South Wales, Sydney, NSW 2052, Australia*

Accepted 2013 November 7. Received 2013 November 5; in original form 2013 October 11

ABSTRACT

In this work, we carry out an analysis of the observed times of primary and secondary eclipses of the post-common envelope binary NSVS 14256825. Recently, Almeida, Jablonski and Rodrigues proposed that two circumbinary companions orbit this short-period eclipsing binary, in order to explain observed variations in the timing of mutual eclipses between the two binary components. Using a standard weighted least-squares minimization technique, we have extensively explored the topology of χ^2 parameter space of a single planet model. We find the data set to be insufficient to reliably constrain a one-companion model. Various models, each with similar statistical significance, result in substantially different orbital architectures for the additional companion. No evidence is seen for a second companion of planetary nature. We suspect insufficient coverage (baseline) of timing data causing the best-fitting parameters to be unconstrained.

Key words: binaries: eclipsing – stars: individual: NSVS 14256825.

1 INTRODUCTION

The discovery of planets within binary star systems has recently sparked an increased interest in their formation, occurrence frequency and dynamical evolution (Portegies Zwart 2013). Several techniques exist to detect additional bodies accompanying binary stars. In addition to the traditional radial velocity technique, Han (2008) outlines the possibility to infer such planets from microlensing observations. Recently, transiting circumbinary planets have been detected using the *Kepler* space telescope (Doyle et al. 2011; Orosz et al. 2012a,b; Welsh et al. 2012; Kostov et al. 2013; Schwamb et al. 2013). Furthermore, companions can be detected from pulsar timing measurements (Wolszczan & Frail 1992). The formation and dynamical evolution of planets around binary star systems have been the subject of recent theoretical studies (Quintana & Lissauer 2006; Haghighipour & Raymond 2007; Marzari et al. 2009; Shi et al. 2012).

Utilizing ground-based observations, a number of multiplanet systems around short-period eclipsing binary stars have been proposed in recent years (Lee et al. 2009; Beuermann et al. 2010; Potter et al. 2011; Qian et al. 2011). From measuring the times at minimum light (either primary and/or secondary eclipse), one can use the light-travel time (LTT) effect to detect additional companions by measuring periodic changes in the binary period (Irwin 1952; Hinse et al. 2012a; Horner et al. 2012a). In contrast to other detection methods (radial velocity, microlensing and transit), the LTT technique is sensitive to massive companions on a long-period orbit: the semi-amplitude K of the LTT signal scales with the companions mass and period as $K \sim M_3$ and $K \sim P_3^{2/3}$, respectively. In addition, low-mass binary components will favour the detection of low-mass companions on short-period orbits (Pribulla et al. 2012).

From ground-based photometric observations, the first two-planet circumbinary system (HW Virginis, a.k.a HW Vir) was proposed by Lee et al. (2009). Additional multibody systems of planetary nature were subsequently proposed by Beuermann et al. (2010); Marsh et al. (2013) (NN Serpentis, a.k.a NN Ser), Potter et al. (2011) (UZ Fornacis, a.k.a. UZ For) and Qian et al. (2011) (HU Aquarii, a.k.a. HU Aqr). Recently, Lee et al. (2012) proposed a quadruple system with two circumbinary sub-stellar companions orbiting the Algol-type binary SZ Hercules (a.k.a. SZ Her).

For a secure detection of a multiplanet circumbinary system, at least two criteria need to be satisfied. First, any period variation, due to additional companions, must be recurring and periodic in time. The data should extend over at least two complete cycles of the longest period. Secondly, the proposed system should be dynamically stable on time-scales comparable to the age of the binary components. Horner et al. (2011) first studied the dynamical stability of the two planets in HU Aqr. Their study allowed them to conclude that the system is highly unstable with disruption times of a few hundred years. Subsequent studies of the same system were carried out by Hinse et al. (2012a), Wittenmyer et al. (2012) and Goździewski et al. (2012). The overall conclusion of these studies is that the planets, as proposed in the discovery work, are

⋆ E-mail: tchinse@gmail.com

simply not feasible. More observational data is necessary before any further constraints can be imposed on the orbital parameters of any companions in the HU Aqr system.

The proposed planets orbiting the close binary system HW Vir (Lee et al. 2009) is another case where the proposed planets do not stand up to dynamical scrutiny (Horner et al. 2012b). In that case, the dynamical character of the HW Vir system was studied, and the planets proposed were found to follow highly unstable orbits most likely due to their crossing orbit architecture and relatively high masses. However, Beuermann et al. (2012b) presented new timing measurements of HW Vir allowing them to conclude stable orbits under the assumption of fixing some of the orbital elements in their least-square analysis.

The NN Ser system was also recently studied by Horner et al. (2012a). These authors found stable orbits for the Beuermann et al. (2010) solutions, if the planets are locked in a mean-motion resonant (MMR) configuration. However, an in-depth remodelling of the timing data renders the system unstable when all parameters are allowed to vary freely. Very recently, Beuermann, Dreizler & Hessman (2013) published additional timing data of NN Ser. Their re-analysis allowed them to conclude the existence of two companions orbiting the binary pair involved in a 2:1 MMR.

Unstable orbits in proposed multibody circumbinary systems have not only been found among companions of planetary nature. The SZ Her system with two sub-stellar mass companions was recently investigated within a dynamical analysis (Hinse et al. 2012b). Here, the authors also found that the proposed companions followed highly unstable orbits.

In a recent work, Almeida et al. (2013) interpreted observed eclipse timing variations of the post-common envelope binary NSVS 14256825 as being the result of a pair of LTT effect introduced by two unseen circumbinary companions. The proposed companions are of planetary nature, with orbital periods $\simeq$3.5 and $\simeq$6.7 yr, and masses of $3\,M_{\rm jup}$ and $8\,M_{\rm jup}$, respectively. Once again, however, a recent study (Wittenmyer, Horner & Marshall 2013) reveals that the proposed planetary system would be dynamically unstable on very short time-scales – with most plausible orbital architectures being unstable on time-scales of just a few hundred years, and only a small fraction of systems surviving on time-scales of 10^5 yr.

The aim of this paper is as follows. In Section 2, we present the available timing data of NSVS 14256825, which forms the basis of our analysis. In particular, we augment the timing measurements presented in Almeida et al. (2013) with three additional data points presented in Beuermann et al. (2012a). We also introduce the LTT model using Jacobian coordinates and outline the derivation of the minimum mass and projected semimajor axis for a single circumbinary companion along with a short description of our least-squares minimization methodology. In Section 3, we carry out a data analysis and perform a period analysis based on Fourier techniques and present our results describing the main properties of our best-fitting solutions. In particular, we present results from finding a best-fitting linear, best-fitting quadratic and best-fitting one-companion model. Finally, we summarize our results and discuss our conclusion in Section 4.

2 DATA ACQUISITION AND JACOBIAN LTT MODEL

As the basis of this work, we consider the same timing data set as published in Almeida et al. (2013). However, we noticed that three timing measurements published in Beuermann et al. (2012a) were not included in Almeida et al. (2013). We have therefore carried out two independent analysis based on the following data sets. Data set I: data as presented in table 3 in Almeida et al. (2013). This data set spans the period from 2007 June 22 to 2012 August 13, corresponding to an observing baseline of around 5 yr. Data set II: data as presented in table 3 in Almeida et al. (2013) *plus three data points* (primary eclipse) from Beuermann et al. (2012a). The additional points are as follows. BJD 245 1339.803 273 $\pm$ 0.000 429 d, BJD 245 2906.673 899 $\pm$ 0.000 541 d and BJD 245 3619.579 776 $\pm$ 0.000 537 d. The second data set spans the period from 1999 June 10 to 2012 August 13, corresponding to an observing baseline of around 13 yr (i.e. doubling the time window).

The aim of considering the second data set (Data set II) is to investigate the effect of the additional timing data on the overall best-fitting solution and compare the results obtained from considering the first data set (Data set I) since it covers a longer observing baseline.

The time stamps in Beuermann et al. (2012a) are stated using the terrestrial time (TT) standard while the times in Almeida et al. (2013) states timing measurements in the barycentric dynamical time (TDB) standard. However, the difference between these time standards (TT versus TDB) introduces timing differences on a millisecond (approx. 0.002 s) level due to relativistic effects (Eastman, Siverd & Gaudi 2010). In light of the quoted measurement uncertainties (from the literature) of the eclipse timings in the two data sets, the two time stamps (TT and TDB) can be combined and no further transformation of one time standard to the other is necessary.

Considering the binary as an isolated two-body system and in the absence of mechanisms that cause period variations, the linear ephemeris of future (or past) eclipses $T_{\rm ecl}$ is given by (Hilditch 2001)

$$T_{\rm ecl}(E) = T_0 + E \times P_0, \tag{1}$$

where E denotes the cycle number, T_0 is the reference epoch and P_0 is the nominal binary period. Additional effects that cause variations of the binary period would be observed as a systematic residual about this best-fitting line.

We use the formulation of the LTT effect based on Jacobian coordinates (Goździewski et al. 2012). In the general case, a circumbinary N-body system is a hierarchical system and employing Jacobian elements therefore seems natural. This is particularly true for the case of a single companion (the first object in a hierarchical multibody ensemble), where the Jacobian coordinate is equivalent to astrocentric coordinates and readily returns the geometric osculating orbital elements of the companion relative to the binary. Here, we assume the binary to be a single massive object with mass equivalent to the sum of the two component masses. For a single circumbinary companion, the LTT signal can be expressed as (Goździewski et al. 2012)

$$\tau(t) = -\frac{\zeta_1}{c}, \tag{2}$$

where c is the speed of light and ζ_1 is given as

$$\zeta_1(t) = K_1 \left[\sin\omega_1(\cos E_1(t) - e_1) + \cos\omega_1 \sqrt{1-e_1^2}\sin E_1(t) \right], \tag{3}$$

Here e_1 denotes the orbital eccentricity and ω_1 measures the argument of pericentre of the companion relative to the combined binary representing the dynamical centre. The eccentric anomaly is given

as E_1. Following Goździewski et al. (2012), the semi-amplitude of the LTT signal is given as

$$K_1 = \left(\frac{1}{c}\right) \frac{m_1}{m_* + m_1} a_1 \sin I_1, \quad (4)$$

with c measuring the speed of light, a_1 the semimajor axis, I_1 the inclination of the orbit relative to the skyplane. The quantities m_* and m_1 denote the masses of the combined binary and companion, respectively.

In summary, the set (K_1, P_1, e_1, ω_1, T_1) represent the five free osculating orbital parameters for the companion with P_1 and T_1 denoting the orbital period and time of pericentre passage, respectively. These latter two quantities are introduced implicitly via *Kepler*'s equation and the eccentric anomaly (Goździewski et al. 2012; Hinse et al. 2012a)

2.1 Deriving minimum mass and projected semimajor axis

Once a weighted least-squares best-fitting model has been found the minimum mass of the companion is obtained from solving the following transcendental function

$$f(m_1) = \gamma_1 (m_1 + m_*)^2 - m_1^3 = 0, \quad (5)$$

where

$$\gamma_1 = \left(\frac{c^3}{k^2}\right) \left(\frac{4\pi^2}{P_1^2}\right) K_1^3. \quad (6)$$

The projected minimum (with $\sin I_1 = 1$) semimajor axis (a_1) is then found from Kepler's third law

$$\frac{P_1^2}{a_1^3} = \frac{4\pi^2}{\mu_1}, \quad (7)$$

where the gravitational parameter is given by $\mu_1 = k^2(m_* + m_1)$ with k denoting Gauss' gravitational constant. The combined mass of the two binary components is assumed to be $m_* = 0.528\,\mathrm{M}_\odot$ (Almeida et al. 2013).

Considering only the case of a single circumbinary companion, the timings of minimum light for primary eclipses is given as

$$T_{\mathrm{ecl}}(E) = T_0 + E \times P_0 + \tau(K_1, P_1, e_1, \omega_1, T_1). \quad (8)$$

We therefore have a total of seven model parameters describing the LTT effect caused by a single circumbinary companion. For a description of two companions, we refer to Goździewski et al. (2012). The LTT signal is a one-dimensional problem similar to the radial velocity technique. We therefore only derive the minimum mass and minimum (projected) semimajor axis of the companion. For simplicity, we henceforth write m_1 and a_1 for the minimum masses and minimum semimajor axis of the companion.[1]

It is worth pointing out that no gravitational interactions have been taken into account in the above formulation of the LTT signal. Only Keplerian motion is considered. It is possible to include additional effects (such as mutual gravitational interactions) that can cause period variations and we refer to Goździewski et al. (2012) for more details.

Finally, we stress that the case of a *single* companion the Jacobian-based description of the one-companion LTT effect is equivalent to the formulation given in Irwin (1952, 1959). Hence, the P_1, e_1, ω_1, T_1 should be identical to those parameters obtained using the Irwin (1952) LTT model along with the derived minimum mass. The only parameter which is different is the semimajor axis of the binary due to the different reference systems used and we refer the reader to Goździewski et al. (2012) for details. For consistency, we tested our results for the presently (Jacobian) derived LTT formulation using the procedure detailed in Irwin (1952), and obtained identical results. However, one complication could arise in the argument of pericentre which can differ depending on the defined direction of the line-of-sight axis. Either this axis can point towards or away from the observer. The difference will affect the argument of pericentre and can be rectified using the relation $\omega_1 = \omega' + \pi$, where ω' is the argument of pericentre defined in a reference system with opposite line-of-sight direction compared to the formulation outlined in Goździewski et al. (2012). Hence the difference is only a matter of convention and does not affect the quantitative results obtained from the two formulations.

2.2 Weighted least-squares fitting

We have implemented the Jacobian-based *Kepler*-kinematic LTT model in IDL.[2] The Levenberg–Marquardt (LM) least-square minimization algorithm was used to find a best-fitting model and is available via the MPFIT routine (Markwardt 2009). We quantify the goodness-of-fit statistic as

$$\chi^2 = \sum_{i=1}^{N} \left(\frac{O_i - C_i}{\sigma_i}\right)^2, \quad (9)$$

where N is the number of data points, $O_i - C_i$ measures the vertical difference between the observed data and the computed model at the ith cycle, and σ_i measures the 1σ timing uncertainty (usually obtained formally). However, in this work we will quote the *reduced* χ^2 defined as $\chi^2_\nu = \chi^2/\nu$ with $\nu = N - n$ denoting the degree of freedom. The MPFIT routine attempts to minimize χ^2 iteratively using n free parameters.

In the search for a global minimum $\chi^2_{\nu,0}$ of the underlying χ^2 space, we utilize a Monte Carlo approach by generating a large number (5×10^5) of random initial guesses. Two approaches can be used to explore the χ^2 space for a global minimum. The first involves generating random initial guesses in a relatively narrow region of a given parameter and may be applied when information about the periodicity and amplitude of the LTT signal is inferred from other means (e.g. Fourier analysis). For example, if a Fourier analysis reveals a given frequency within the data one can then generate random initial guesses from a normal distribution centred at that period with some (more or less narrow) standard deviation for the variance. In the second approach, random initial guesses are generated from a uniform distribution defined over a broad interval for a given parameter. However, in both approaches we randomly choose the eccentricity from a uniform distribution within $e_1 \in [0, 0.99]$ with the argument of pericentre chosen from $\omega_1 \in [-\pi, \pi]$. In all our searches, we recorded the initial guess and final parameters along with the goodness-of-fit value, the corresponding root-mean-square (rms) statistic and formal 1σ uncertainties. A single LM iteration sequence is terminated following default values of accuracy parameters within MPFIT or after a maximum of 3000 iterations (rarely encountered with the average number of iterations required being just 11).

[1] Technically, the values obtained represent the minimum possible values of $m_1 \sin I_1$ and $a_1 \sin I_1$ – but in standard papers dealing with eclipse timing or radial velocity studies authors use the shortened versions, for brevity.

[2] http://www.exelisvis.com/ProductsServices/IDL.aspx

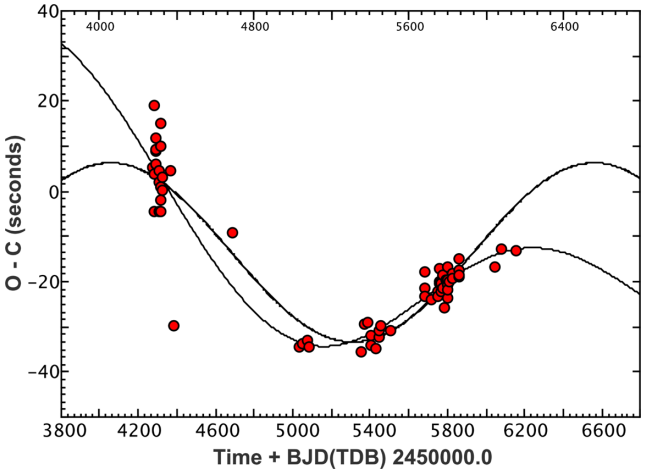

Figure 1. Graphical result from PERIOD04 analysis performed on Data set I showing two graphs with one or two Fourier components. The general form follows $O - C = \sum A_i \sin(2\pi(\omega_i t + \phi_i))$. The first component has $A_1 = 19.85$ s, $\omega_1 = 3.99 \times 10^{-4}$ cycles d^{-1} (corresponding to a period of 6.9 yr) and $\phi_1 = 0.63$ radians. The second component has $A_2 = 33.37$ s, $\omega_2 = 1.33 \times 10^{-4}$ cycles d^{-1} (period of 20.6 yr) and $\phi_2 = 0.93$ radians.

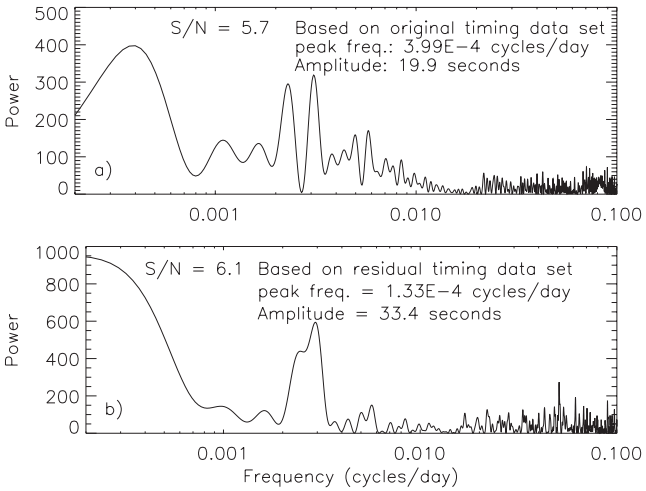

Figure 2. Power spectrum of the NSVS 14256825 timing data with the linear part (from a linear regression) subtracted. Additional peaks correspond to $\simeq$1 yr alias frequencies originating from the annual observing cycle.

3 DATA ANALYSIS AND RESULTS

3.1 Period analysis and linear ephemeris

As a starting point for our analysis, we first determined the parameters of the linear ephemeris (T_0, P_0) by calculating a linear least-squares regression line to the same data (Data set I) as considered by Almeida et al. (2013). A best-fitting line resulted in a $\chi^2_{65} \simeq 13$ with $n = 2$ free parameters and $N = 67$ data points. The corresponding χ^2 value was found to be 853 and the (rounded) linear ephemeris was determined to be

$$T^I_{\rm ecl} = T_0 + E \times P_0 \tag{10}$$

$$= \mathrm{BJD}\ 245\,5408.744\,502 \pm 3 \times 10^{-6} + E \times 0.110\,374\,1881 \pm 8 \times 10^{-10}\ \mathrm{d} \tag{11}$$

$$= \mathrm{BJD}\ 245\,5408.744\,502^{505}_{499} + E \times 0.110\,374\,1881^{89}_{73}\ \mathrm{d}. \tag{12}$$

For Data set II, we obtained the slightly different ephemeris, with little improvement in the precision of the binary period

$$T^{II}_{\rm ecl} = T_0 + E \times P_0 \tag{13}$$

$$= \mathrm{BJD}\ 245\,5408.744\,504 \pm 3 \times 10^{-6} + E \times 0.110\,374\,1759 \pm 8 \times 10^{-10}\ \mathrm{d} \tag{14}$$

$$= \mathrm{BJD}\ 245\,5408.744\,504^{507}_{501} + E \times 0.110\,374\,1759^{67}_{51}\ \mathrm{d}. \tag{15}$$

We applied the PERIOD04[3] (Lenz & Breger 2005) Lomb–Scargle algorithm on the residual data (Fig. 1) obtained from subtracting the best-fitting line, and compared two fits to the residual data. The first had a single Fourier component, whilst the second had two Fourier components as shown in Fig. 1. The two-component fit was found to provide a better description of the data. We show the corresponding power spectra in Fig. 2, and find the 6.9 yr period to be in agreement with the period found by Almeida et al. (2013). However, the algorithm was unable to detect the 3.5 yr cycle (inner proposed planet) as determined in Almeida et al. (2013). Instead, we found a 20.6 yr cycle with a detection six times above the noise level.

[3] http://www.univie.ac.at/tops/Period04/

3.2 Quadratic ephemeris model – Data set I

In some cases, a change of the binary period can be caused by non-gravitational interaction between the two components of a short-period eclipsing binary. Often the period change is described by a quadratic ephemeris (linear plus secular) with the times of primary eclipses given by Hilditch (2001)

$$T_{\rm ecl}(E) = T_0 + P_0 \times E + \beta \times E^2, \tag{16}$$

where β is a period damping factor (Goździewski et al. 2012) which can account for mass-transfer, magnetic braking, gravitational radiation and/or the influence of a distant companion on a long-period orbit. Following Brinkworth et al. (2006), the rate of period change, in the case of mass-transfer, is then given by

$$\dot{P} = \frac{2\beta}{P}, \tag{17}$$

with P denoting the currently measured binary period. In Fig. 3, we show the best-fitting quadratic ephemeris given as

$$T_{\rm ecl}(E) = (\mathrm{BJD}\ 245\,5408.744\,485 \pm 3.4 \times 10^{-6}) + (0.110\,374\,1772 \pm 8.9 \times 10^{-10}) \times E \tag{18}$$

$$+ (3.1 \times 10^{-12} \pm 1.4 \times 10^{-13}) \times E^2 \tag{19}$$

with unreduced $\chi^2 = 360$ for (67–3) degrees of freedom. In Fig. 4, we show the location of the best-fitting surrounded by the 1σ (68.3 per cent, $\Delta\chi^2 = 2.3$), 2σ (95.4 per cent, $\Delta\chi^2 = 6.2$) and 3σ (99.7 per cent, $\Delta\chi^2 = 18.4$) joint-confidence contours (Press et al. 2002; Bevington & Robinson 2003; Hughes & Hase 2010) for the (P_0, β) parameter space. Similar results were obtained for the remaining two parameter combinations. Considering Data set I, we found the average period change to be $\dot{P} = 5.6 \times 10^{-11}$ s s^{-1}. This value is about one order of magnitude smaller than the period decrease reported in Almeida et al. (2013).

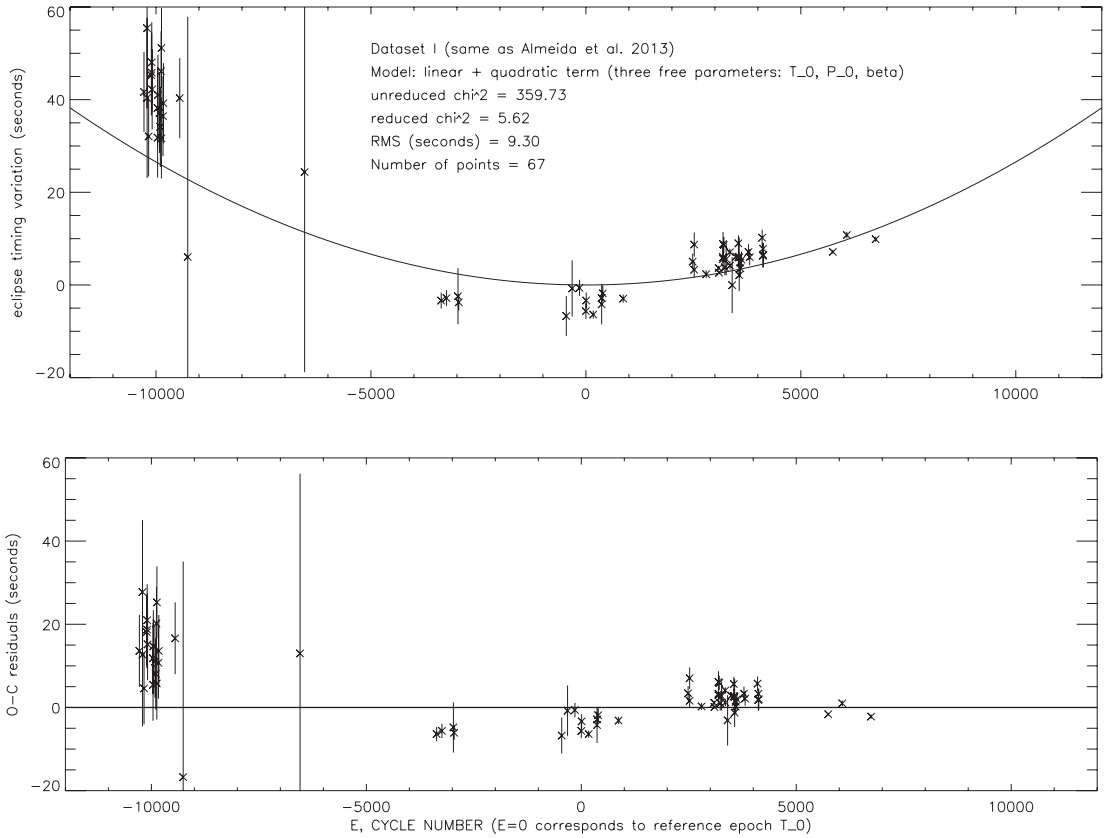

Figure 3. Quadratic ephemeris model to Data set I. Best-fitting parameters (T_0, P_0, β) along with their formal uncertainties are listed in Section 3.2. The loci of points at $E = -10\,000$ appear to be systematically off-set by $+15$ s from the expected parabola. The root-mean-square scatter around the parabola is around 9 s.

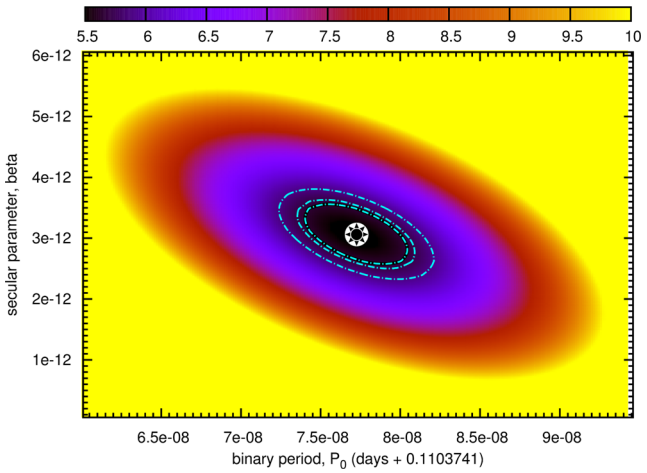

Figure 4. Colour-coded χ^2_ν scans for the quadratic ephemeris model (Fig. 3). The β parameter denotes the period damping factor. Remaining parameters were allowed to vary freely. The best-fitting solution is shown by a star-like symbol. Contour curves (from inner to outer) show the $1-$, $2-$, $3-\sigma$ confidence levels around the best-fitting model (symbol). See the text for more details.

3.3 Single companion model – Data set I

To reliably assess the validity of a two-companion model, we first considered a one-companion model. Our period analysis yielded a shortest period of around $P_1 \simeq 7$ yr (2557 d) with a semi-amplitude of $K_1 \simeq 0.000\,231$ d (20 s). We therefore searched for a best-fitting solution in a narrow interval around these values by seeding 523 110 initial guesses. The best-fitting solution with $\chi^2_{60,0} = 1.98$ is shown in Fig. 5. In Table 1, we show the corresponding best-fitting parameters and derived quantities for the companion along with their formal (derived from the covariance matrix) 1σ uncertainties as obtained from MPFIT. Formal errors in the derived quantities were obtained from numerical error propagation, as described in Bevington & Robinson (2003). The residual plot in Fig. 5 (middle panel) shows no obvious trend above the 5 s level. The average timing uncertainty in the Almeida et al. (2013) data set is 5.5 s. An additional signal associated with an LTT effect should be detected on a 3σ level equivalent to a timing semi-amplitude of $\simeq$15 s. Usually timing measurement are assumed to distribute normally around the expected model. We have therefore also plotted the normalized residuals $(O_i - C_i)/\sigma_i$ (Hughes & Hase 2010) as shown in the bottom panel of Fig. 5. The corresponding histogram is shown in Fig. 6. Whether the timing residuals follow a Gaussian distribution is unclear at the moment.

Again, we have explored the χ^2_{60} function in the vicinity of the best-fitting parameters and determined two-dimensional joint-confidence intervals. We show all 21 two-parameter combinations in Figs 7 and 8. While the two considered parameters in a given panel were kept fixed, we allowed all the remaining parameters to re-optimize (with an initial guess given by the best-fitting values listed in Table 1) during an LM iteration (Bevington & Robinson 2003).

We note that several of the parameters correlate with each other. This is especially true for the (T_1, ω_1) pair shown in Fig. 8. Choosing our reference epoch T_0 to be close to the middle of the data set results

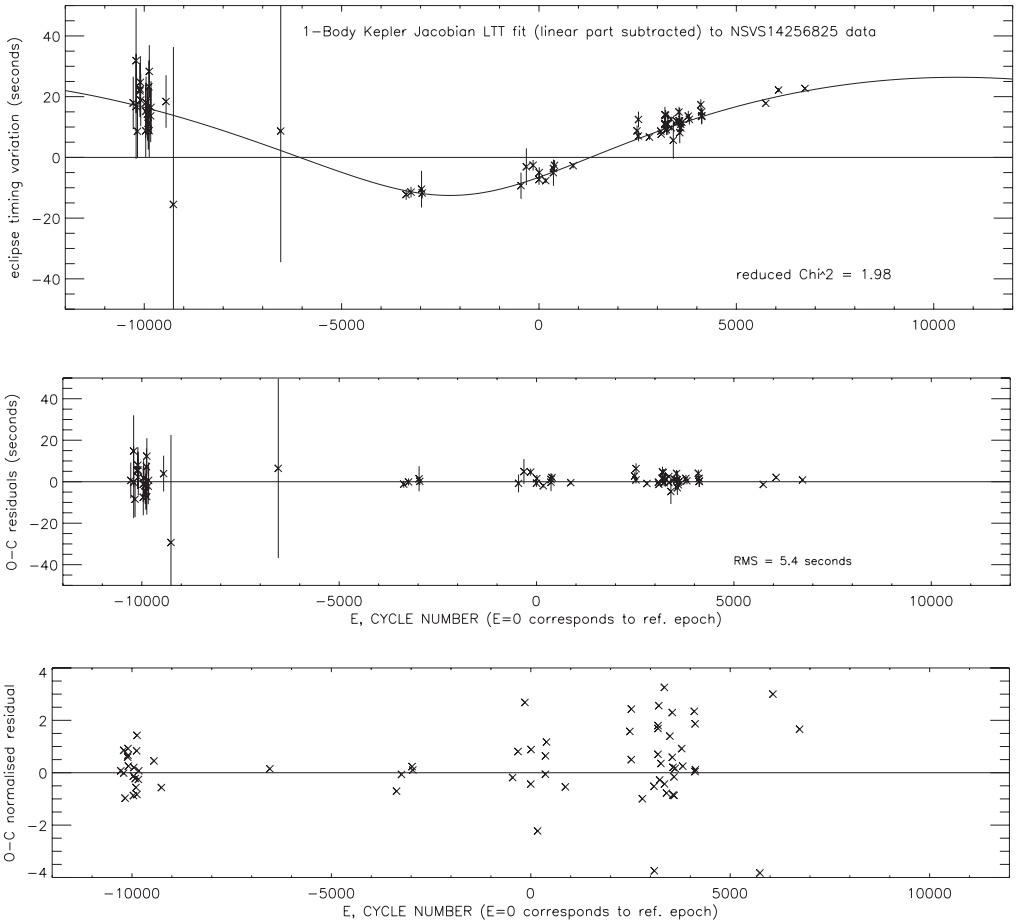

Figure 5. Best-fitting model (top panel) to the timing data as considered by Almeida et al. (2013). We subtracted the linear part. Middle panel: residuals $O_i - C_i$ versus cycle number with a root-mean-square scatter (rms) of about 5 s. Bottom panel: plot of normalized residuals $(O_i - C_i)/\sigma_i$ (dimensionless, see the text) between observed and computed times.

Table 1. Best-fitting parameters for the one-companion LTT model of NSVS 14256825 corresponding to Fig. 5. rms measures the rms scatter of the data around the best-fitting model. We quote formal uncertainties obtained from the covariance matrix provided by MPFIT. Uncertainties for the minimum mass and semimajor axis (relative to the binary mass centre) of the companion were derived via error propagation (Bevington & Robinson 2003).

Data set I		
$\chi^2_{60,0} = 1.98, N = 67, n = 7, \nu = 60$		
rms	5.4	s
T_0	245 5408.744 50(36)	BJD
P_0	0.110 374 15(5)	d
K_1	$0.000\,23 \pm 0.000\,05$	au
e_1	0.3 ± 0.1	–
ω_1	1.7 ± 0.3	r
T_1	245 5197(67)	BJD
P_1	2921 ± 258	d
$m_1 \sin I_1$	6.7 ± 0.9	$M_{\rm jup}$
$a_1 \sin I_1$	3.3 ± 0.6	au
e_1	0.3 ± 0.1	–
ω_1	$(1.7 + \pi) \pm 0.3$	r
P_1	2921 ± 258	d

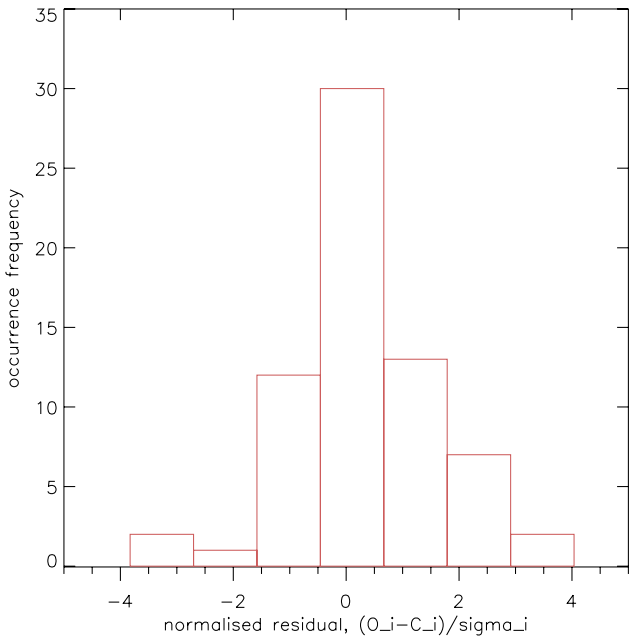

Figure 6. Occurrence frequency of normalized residuals (bottom panel in Fig. 5) resembling a somewhat symmetric normal distribution. The units on the first axis are standard deviations with $1\sigma \simeq 5$ s. The bin size was chosen to be 1.2σ.

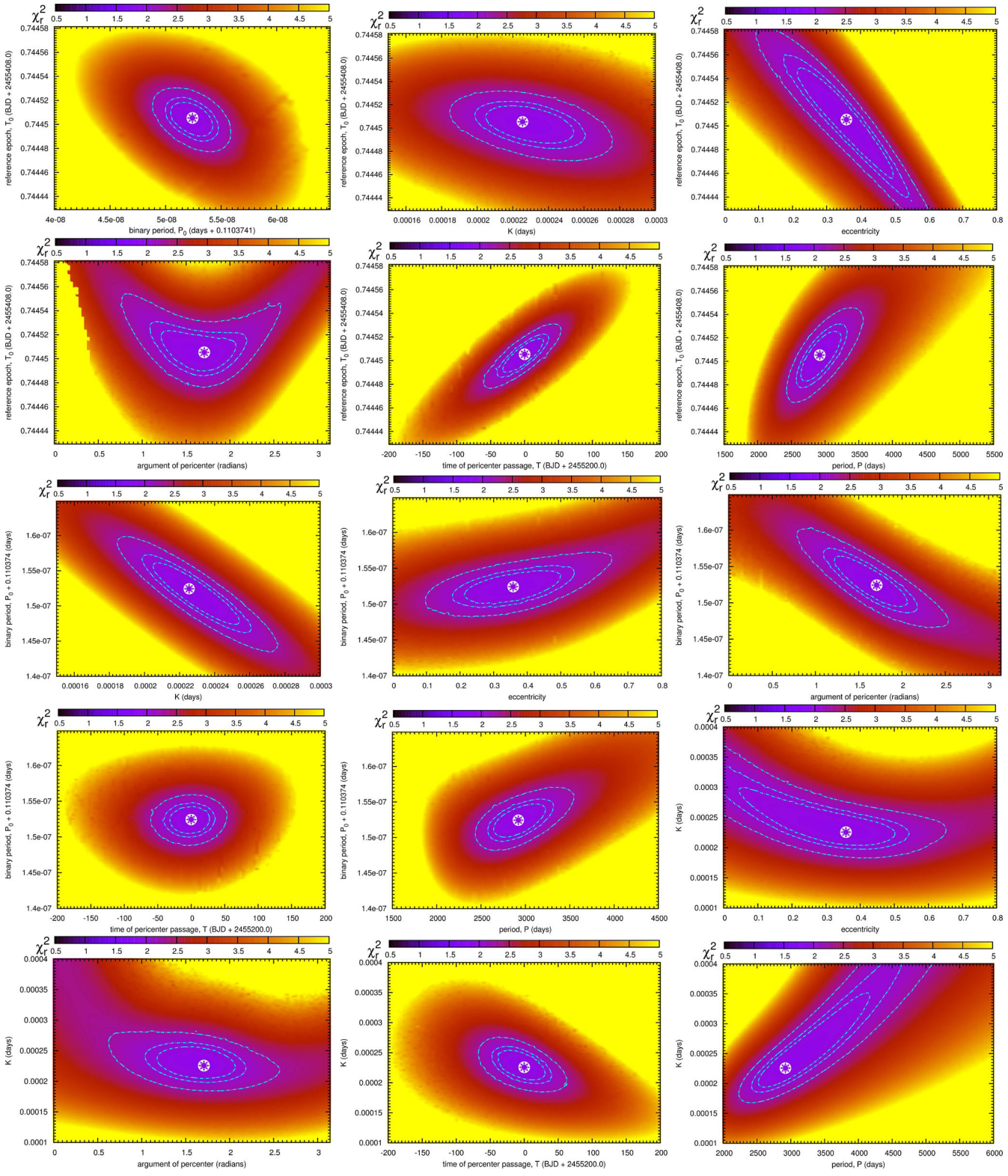

Figure 7. Similar to Fig. 4 but showing scans of orbital parameters for the linear + one-LTT model.

in almost no correlation between T_0 and P_0 (see top-left panel in Fig. 7). In addition, we note that the χ^2 topology around the best-fitting parameters deviates from its expected parabolic form. This is most readily apparent in the (ω_1, e_1) panel in Fig. 8.

Finally, we note that the 3σ confidence level in the (P_1, K_1) (bottom-right) panel of Fig. 7 appears open, and stretches towards longer periods (P_1) and larger semi-amplitudes (K_1). With this in mind, we then recalculated the χ^2 space of (P_1, K_1) considering a

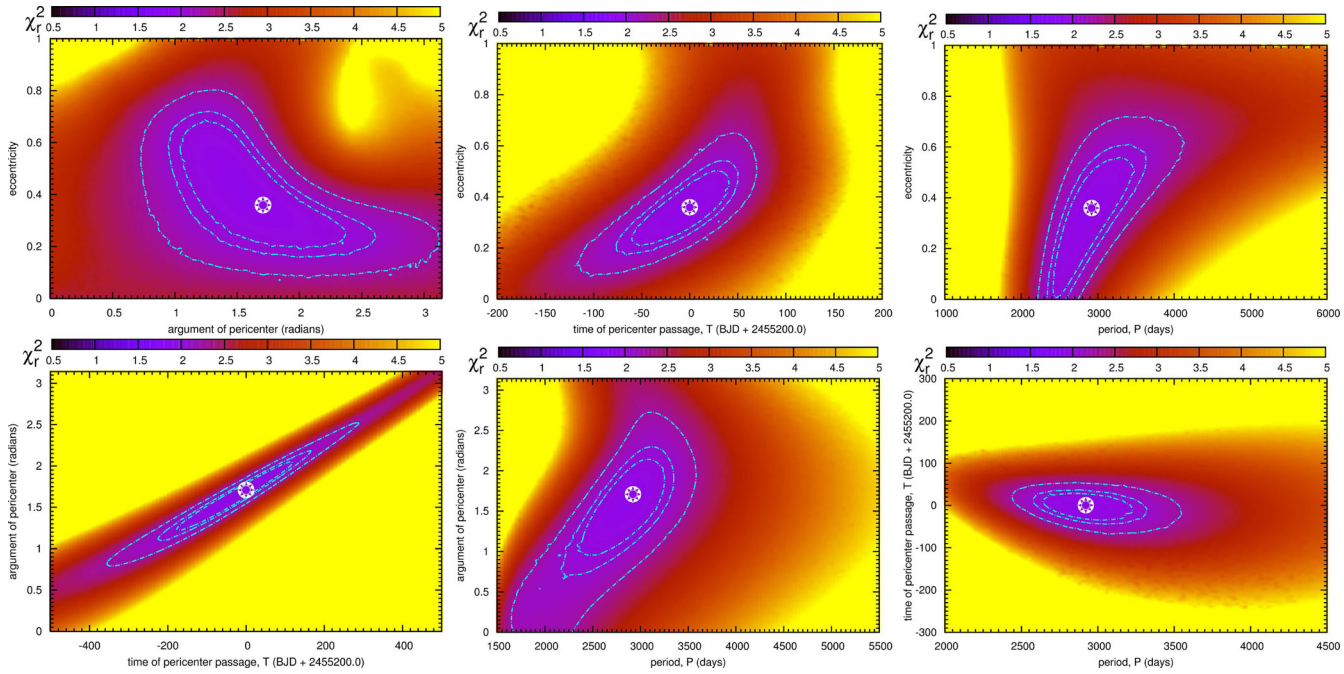

Figure 8. Similar to Fig. 7 but for the remaining six parameter combinations.

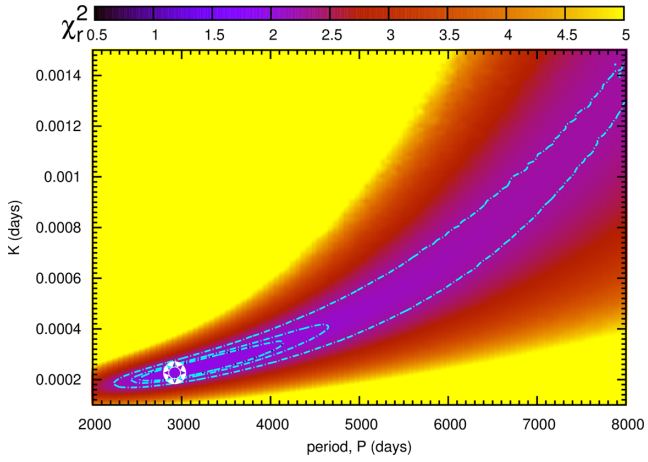

Figure 9. Best-fitting solution and the result of calculating the two-dimensional joint-confidence contours of a single-companion model over a larger parameter interval.

larger interval in the two parameters. The result is shown in Fig. 9, demonstrating that the 3σ joint-confidence contour remains open for orbital periods larger than around 22 yr. We therefore suspect that our best-fitting model resides within a local minimum.

To test whether we are dealing with a local minimum, we explore the χ^2 parameter space on a wider search grid by following the approach as outlined previously. Surprisingly, we found a marginally improved solution with a smaller best-fitting $\chi^2_{60,0*}$ value of 1.96, a reduction by 2 per cent compared to the first best-fitting solution of 1.98. Computing the χ^2_{60} space around the new best-fitting solution over a large interval in the parameters K_1, e_1 and P_1 resulted in Fig. 10.

In each panel, our (new) improved best-fitting solution is marked by a cross-hair. The corresponding model parameters are shown in Table 2. We have omitted quoting the formal uncertainties for reasons that will become apparent shortly. In Fig. 10, we also show the 1σ (68.3 per cent) joint-confidence contour of $\Delta\chi^2_{60} = 1.993$ (black line) encompassing our best-fitting model. Our results suggest that a plethora of models, with χ^2_{60} within the 1σ confidence level, are equally capable of explaining the timing data. Statistically, within the 1σ uncertainty region, essentially no differences in the χ^2 exist between the various solutions.

For this reason, the considered parameters (semi-amplitude, eccentricity and period) span a vast range, making it impossible to place firm confidence intervals on them. From Fig. 10, possible periods span from $\simeq$2500 d (6.8 yr) to at least 80 000 d (219 yr) chosen as our upper cut-off limit in the search procedure. We have tested this result by selecting three significantly different pairs of (P_1, e_1) in Fig. 10(a). We label them as follows: Example (1): $(P_1, e_1) = (3973\,\mathrm{d}, 0.40)$. Example (2): $(P_1, e_1) = (15\,769\,\mathrm{d}, 0.77)$. Example (3): $(P_1, e_1) = (75\,318\,\mathrm{d}, 0.91)$. We re-calculated a best-fitting model with the (P_1, e_1) parameters held fixed, and remaining parameters $(T_0, P_0, K_1, \omega_1, T_1)$ allowed to vary freely (starting from the best-fitting solution given by the cross-hair in Fig. 10a) to find new optimum values. We show the results of this experiment in Fig. 11. All models have χ^2_{60} within the 1σ confidence level (1.993) but differ significantly in their orbital periods, eccentricities and semi-amplitudes. Our best-fitting model (cross-hair) is shown in Fig. 11(d) and Table 2. We calculated the following values for the companion's minimum mass and semimajor axis for our three examples. Example (1): $m_1 \sin I_1 = 7.6\,M_{\mathrm{jup}}$, $a_1 \sin I_1 = 4.0$ au. Example (2): $m_1 \sin I_1 = 8.5\,M_{\mathrm{jup}}$, $a_1 \sin I_1 = 10.0$ au. Example (3): $m_1 \sin I_1 = 9.7\,M_{\mathrm{jup}}$, $a_1 \sin I_1 = 28.4$ au. In light of the large range of possible parameters, we omit quoting parameter uncertainties. Minimum mass and semimajor axis for our improved best-fitting solution (Fig. 11d) are given in Table 2.

Up to this point, our analysis allows us to conclude that the data is not spanning a sufficiently long observing baseline to firmly constrain the parameters of a single companion model. We stress that the model itself could still be valid. With the data currently at hand it is impossible to establish firm confidence intervals on the parameters. Our first solution (comparable with the solution

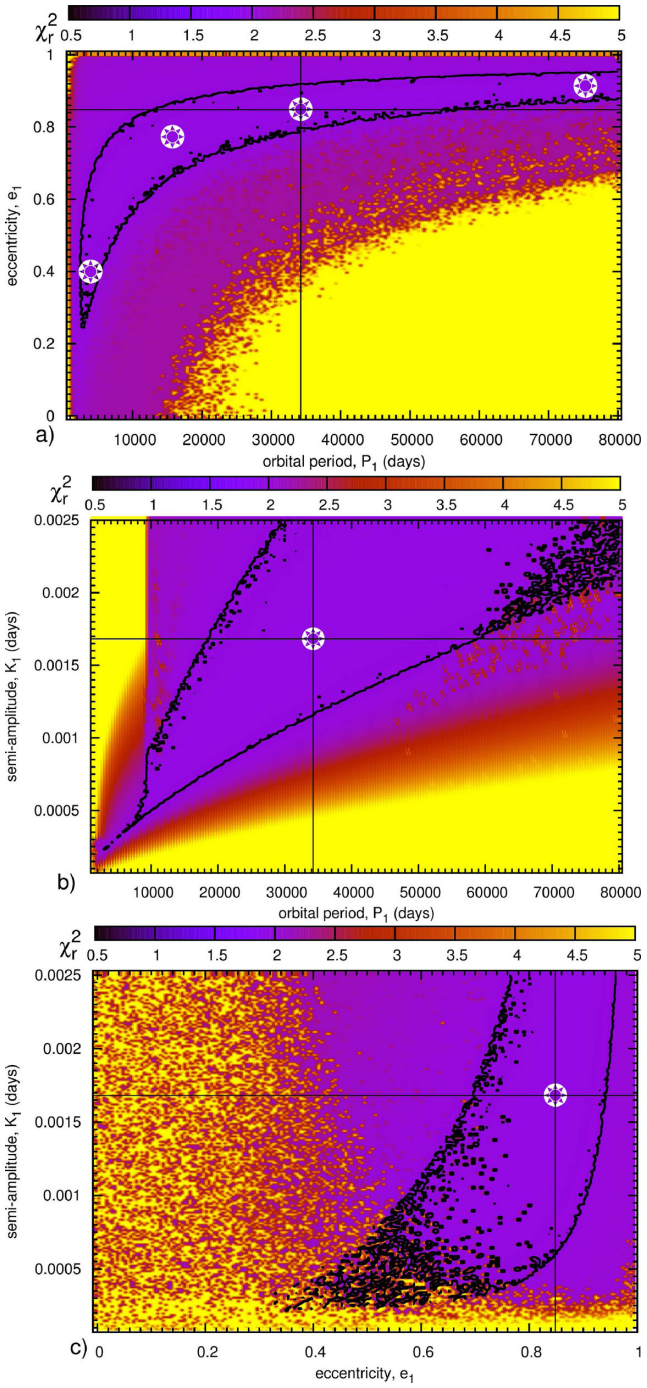

Figure 10. Best-fitting solution (cross-hair) when searching over a large search grid in the period and semi-amplitude. We show the result of calculating the two-dimensional joint-confidence contour with $\Delta\chi^2 = 2.3$ (68.3 per cent). The black contour line is the 1σ confidence level with $\chi^2_{60,0} = 1.993$. In panel (a) we show also three randomly chosen pairs of (P_1, e_1) all within the 1σ level.

presented in Almeida et al. 2013) likely represents a local minimum in the χ^2_ν parameter space, or appears to be a solution within the 1σ confidence interval characterized by a shallow topology of χ^2 space. In such a case, we cannot distinguish isolated models in the continuum of possible solutions. All three panels in Fig. 10 indicate the existence of local minima with χ^2_ν statistics close to our first best-fitting solution with $\chi^2_{60,0} = 1.98$ (Table 1). In fact,

Table 2. Similar to Table 1, but this time the best-fitting (Fig. 11d) is obtained from the extended search case by randomly generated initial guesses from a region spanning a larger interval of the parameters (mainly K_1, e_1 and P_1). In Fig. 10, we show the best-fitting parameters for P_1, e_1 and K_1 as a cross-hair. Formal parameter uncertainties are omitted (see the text for details).

Data set I		
$\chi^2_{60,0} = 1.96, N = 67, n = 7, \nu = 60$		
rms	5.3	s
T_0	245 5408.744 55(41)	BJD
P_0	0.110 374 11(6)	d
K_1	0.001 69	au
e_1	0.85	–
ω_1	2.33	r
T_1	245 5330	BJD
P_1	34 263	d
$m_1 \sin I_1$	9.8	$M_{\rm jup}$
$a_1 \sin I_1$	16.8	au
e_1	0.85	–
ω_1	$(2.33 + \pi)$	r
P_1	34 263	d

Fig. 10 suggests the existence of multiple local minima in the χ^2_ν space. Since in Fig. 10 we have not found the 1σ confidence level to render as a closed-loop contour line, we suspect that the data can be fit to an infinite number of models each having the *same* statistical significance, but exhibiting significant differences in their orbital architectures. In light of this result any efforts to search for a second companion in Data set I seem unfruitful.

3.4 Single companion model – Data set II

We have noted that three data points from Beuermann et al. (2012a) were not included in the analysis presented in Almeida et al. (2013). Although they are accurate (placing them well on the linear ephemeris), their timing precision is lower. However, the large timing uncertainty for these points should not disqualify them from being included in the analysis. In principle, the precision of the eclipsing period P_0 should increase for a data set of increased baseline, and could eventually help to constrain any long-period trend. We have repeated our search procedure as outlined previously to find a best-fitting model based on data set II. We show our best-fitting solution in Fig. 12 and state the best-fitting parameters within the figure area.

For data set II, the main characteristics of the Keplerian orbit for the companion are similar to the parameters shown in Table 2. The period, minimum semimajor axis and eccentricity are comparable in both cases. We also explored the topology of χ^2 space for a large region around the best-fitting solution and found similar results as discussed previously by generating two-dimensional joint-confidence interval maps. The 1σ confidence contour around the best-fitting solution extends over a large interval in the period, eccentricity and semi-amplitude.

From examining the residual plot in Fig. 12, we are not convinced about any additional LTT periodicity above the rms level of about 6 s. An LTT signal with amplitude of around 6 s would require a data

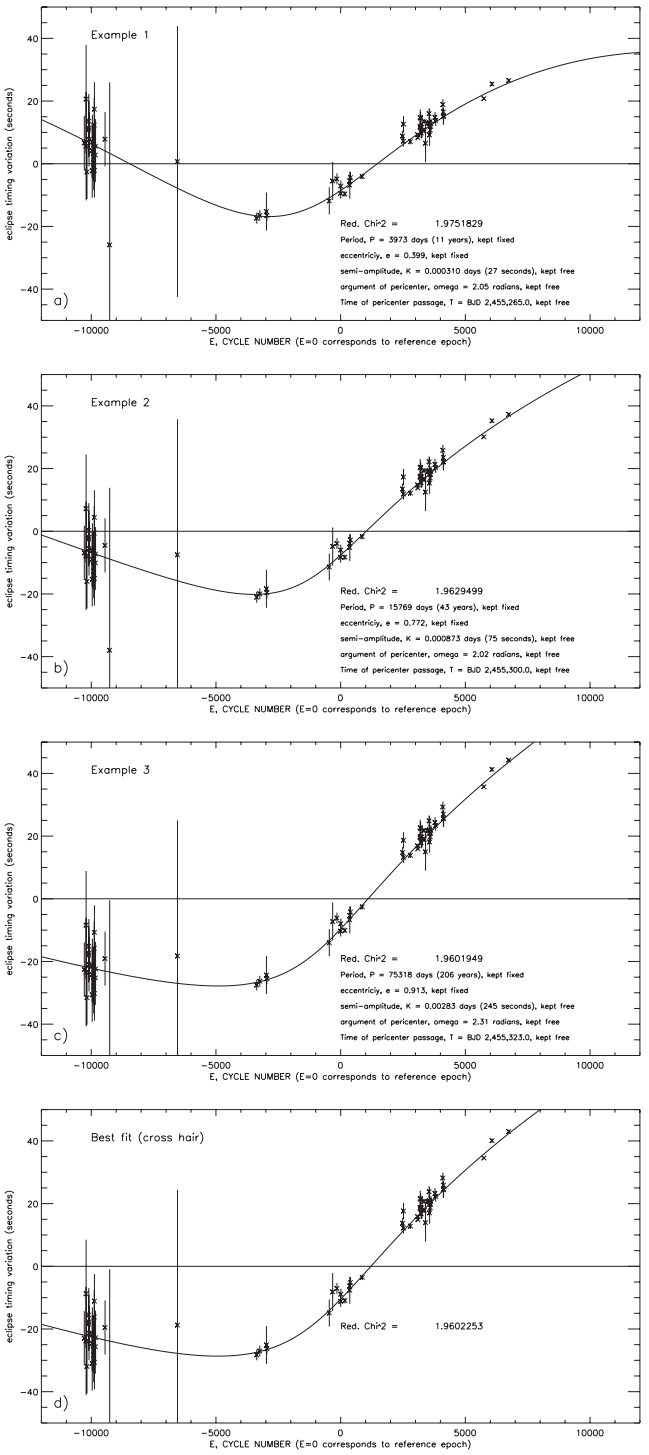

Figure 11. Results of considering various models in Fig. 10. Panels a to c show the models for example 1 to 3. Panel d shows the best-fitting model indicated by a cross-hair in Fig. 10. All models have a reduced χ^2 statistic within the 1σ confidence limit, but the underlying orbital architectures are differing significantly. See the text for more details.

set with rms of about 1 s or less. Hence, from a qualitative judgment, the data in Data set II does not currently support the inclusion of five additional parameters corresponding to a second companion. The results from examining Data set II reinforces insufficient coverage of the orbit as presented in Almeida et al. (2013). Because Data set II covers two-times the best-fitting period found for Data set I, one would expect Data set II to constrain the orbital period to a higher degree than for Data set I. However, this is not the case for the present situation.

4 SUMMARY AND CONCLUSIONS

In this work, we have carried out a detailed data analysis of timing measurements of the short-period eclipsing binary NSVS 14256825. In particular, we have examined the one-companion model bearing in mind that additional valid companions should be readily visible in the resulting residuals. On the basis of Data set I, we first carried out an initial local search for a weighted least-squares best-fitting solution. A best-fitting model (Table 1) with $\chi^2_\nu \simeq 1.98$ resulted in an inner circumbinary companion with orbital characteristics comparable to the short-period companion presented in Almeida et al. (2013). Extending our search grid of χ^2 parameter space resulted in a similar best-fitting χ^2_ν statistic with significantly different orbital characteristics (Table 2). We were able to show quantitatively that the present timing data does not allow us to firmly constrain a particular model with well-established parameter confidence limits. In light of this, quoting formal errors for the model parameters seems meaningless. We concluded that the best-fitting solution found by Almeida et al. (2013) most likely represents a local minimum. We explain the lack of constraint in the parameters by the limited monitoring baseline over which timing data was acquired. Data set I represented a baseline of about 5 yr. If a periodicity is present, the principle of recurrence should apply, requiring two full orbital periods to be covered in order to establish firm evidence for the presence of a companion. This would correspond to an LTT period of at most 2.5 yr for Data set I and 6 yr for Data set II (spanning about 13 yr). However, for Data set I, the data did not allow models with periods shorter than $\simeq$1000 d. Simultaneously Data set II does not constrain the period any better than Data set I.

Our analysis did not allow us to find convincing evidence of a second LTT signal. The rms scatter of timing data around the best-fitting model was found to be around 5 s. Signals with a semi-amplitude comparable with the measurement uncertainties seem unlikely to be supported by the present data. The claimed second companion in Almeida et al. (2013) has a semi-amplitude of $K_2 \simeq 4.9$ s. It is likely that noise was wrongly interpreted as an LTT signal. We recommend that a secure detection requires a signal semi-amplitude of at least three times above the noise level (i.e. $K \simeq 3 \times$ rms). Future timing data (Park et al. 2012; Pribulla et al. 2012) of this system will be important to help constraining the parameters significantly.

ACKNOWLEDGEMENTS

Research by TCH is carried out at the Korea Astronomy and Space Science Institute (KASI) under the 2012 KRCF (Korea Research Council for Science and Technology) Young Scientist Research Fellowship Programme. KG is supported by Polish NSC, grant N/N203/402739. Numerical computations were partly carried out using the SFI/HEA Irish Centre for High-End Computing (ICHEC) and the PLUTO computing cluster at KASI. Astronomical research at Armagh Observatory is funded by the Department of Culture, Arts and Leisure (DCAL). TCH and JWL acknowledges support from KASI grant 2013-9-400-00. JH gratefully acknowledges financial support of the Australian government through ARC Grant DP0774000. RAW is supported by a UNSW Vice-Chancellor's Fellowship.

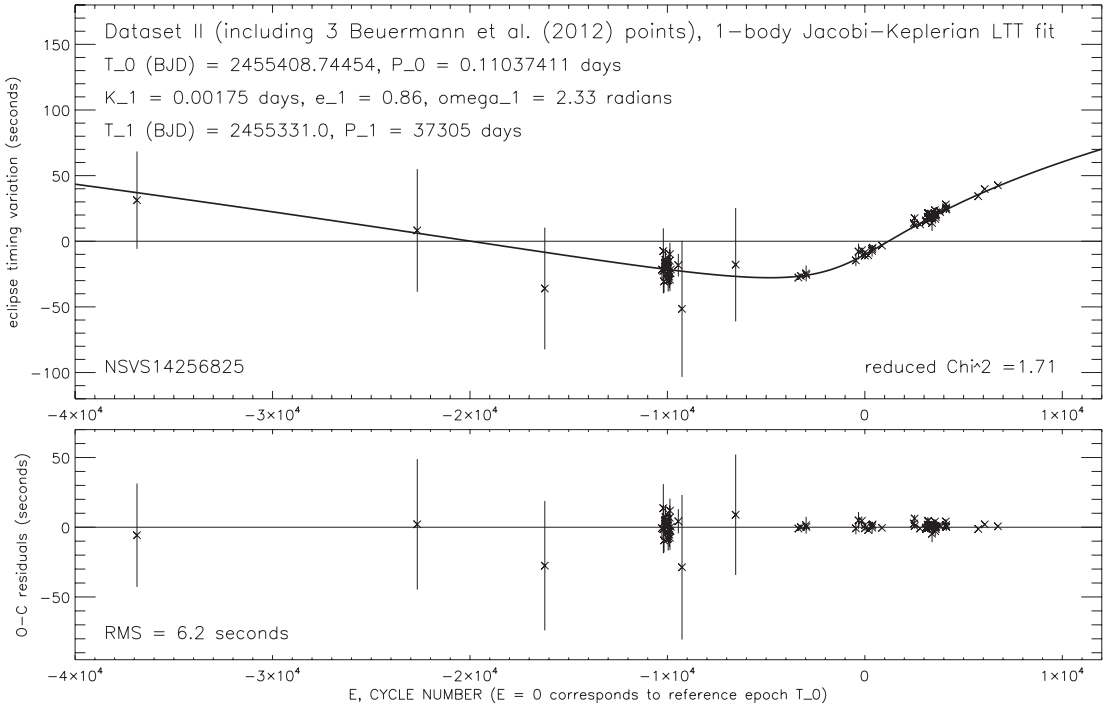

Figure 12. Best-fitting solution based on Data set II (see Section 2). The $\chi^2_{60,0}$ is smaller due to the inclusion of additional three timing measurements by Beuermann et al. (2012a). The residual plot does not support the existence of an additional LTT signal above the root-mean-square (rms) of about 6 s. Signals with a semi-amplitude smaller than 6 s should be treated with caution.

REFERENCES

Almeida L. A., Jablonski F., Rodrigues C. V., 2013, ApJ, 766, 11
Beuermann K. et al., 2010, A&A, 521, L60
Beuermann K. et al., 2012a, A&A, 540, 8
Beuermann K., Dreizler S., Hessman F. V., Deller J., 2012b, A&A, 543, 138
Beuermann K., Dreizler S., Hessman F. V., 2013, A&A, 555, A133
Bevington P. R., Robinson D. K., 2003, Data Reduction and Error Analysis for The Physical Sciences, 3rd edn. McGraw-Hill, USA
Brinkworth C. S., Marsh T. R., Dhillon V. S., Knigge C., 2006, MNRAS, 365, 287
Doyle L. R. et al., 2011, Science, 333, 1602
Eastman J., Siverd R., Gaudi B. S., 2010, PASP, 122, 935
Goździewski K. et al., 2012, MNRAS, 425, 930
Haghighipour N., Raymond S. N., 2007, ApJ, 666, 436
Han C., 2008, ApJ, 676, 53
Hilditch R. W., 2001, An Introduction to Close Binary Stars. Cambridge Univ. Press, UK
Hinse T. C., Lee J. W., Goździewski K., Haghighipour N., Lee C.-U., Scullion E. M., 2012a, MNRAS, 420, 3609
Hinse T. C., Goździewski K., Lee J. W., Haghighipour N., Lee C.-U., 2012b, AJ, 144, 34
Horner J., Marschall J. P., Wittenmyer R., Tinney C. G., 2011, MNRAS, 416, L11
Horner J., Wittenmyer R. A., Hinse T. C., Tinney C. G., 2012a, MNRAS, 425, 749
Horner J., Hinse T. C., Wittenmyer R. A., Marshall J. P., Tinney C. G., 2012b, MNRAS, 427, 2812
Hughes I. G., Hase T. P. A., 2010, Measurements and their Uncertainties - A Practical Guide to Modern Error Analysis. Oxford Univ. Press, UK
Irwin J. B., 1952, ApJ, 116, 211
Irwin J. B., 1959, AJ, 64, 149
Kostov V. B., McCullough P. R., Hinse T. C., Tsvetanov Z. I., Hébrard G., Díaz R. F., Deleuil M., Valenti J. A., 2013, ApJ, 770, 52
Lee J. W., Kim S.-L., Kim C.-H., Koch R. H., Lee C.-U., Kim H. I., Park J.-H., 2009, AJ, 137, 3181
Lee J. W., Lee C.-U., Kim S.-L., Kim H.-I., Park J.-H., 2012, AJ, 143, 34
Lenz P., Breger M., 2005, Commun. Asteroseismol., 146, 53
Markwardt C. B., 2009, in Bohlender D. A., Durand D., Dowler P., eds, ASP Conf. Ser. Vol. 411, Astronomical Data Analysis Software and Systems XVIII. Astron. Soc. Pac., San Francisco, p. 251
Marsh T. R. et al., 2013, MNRAS, pre-print (arXiv:1310.1391)
Marzari F., Scholl H., Thébault P., Baruteau C., 2009, A&A, 508, 1493
Orosz J. A. et al., 2012a, Science, 337, 1511
Orosz J. A. et al., 2012b, ApJ, 758, 87
Park B.-G. et al., 2012, Proc. SPIE, 8444, 47
Portegies Zwart S., 2013, MNRAS, 429, 45
Potter S. B. et al., 2011, MNRAS, 416, 2202
Press W. H., Teukolsky S. A., Vetterling W. T., Flannery B. P., 2002, Numerical Recipies in Fortran90: The Art of Scientific Computing. Cambridge Univ. Press, UK
Pribulla T. et al., 2012, Astron. Nachr., 333, 754
Qian S.-B. et al., 2011, MNRAS, 414, L16
Quintana E. V., Lissauer J. J., 2006, Icarus, 185, 1
Schwamb M. E. et al., 2013, ApJ, 768, 127
Shi J.-M., Krolik J. H., Lubow S. H., Hawley J. F., 2012, ApJ, 749, 118
Welsh W. F. et al., 2012, Nature, 481, 475
Wittenmyer R. A., Horner J., Marshall J. P., Butters O. W., Tinney C. G., 2012, MNRAS, 419, 3258
Wittenmyer R. A., Horner J., Marshall J. P., 2013, MNRAS, 431, 2150
Wolszczan A., Frail D. A., 1992, Nature, 355, 145

This paper has been typeset from a TEX/LATEX file prepared by the author.